Topological phase transition in a discrete quasicrystal

Eran Sagi[*] and Eli Eisenberg

Raymond and Beverly Sackler School of Physics and Astronomy, Tel Aviv University, Tel Aviv 69978, Israel
(Received 13 January 2014; revised manuscript received 9 May 2014; published 3 July 2014)

We investigate a two-dimensional tiling model. Even though the degrees of freedom in this model are discrete, it has a hidden continuous global symmetry in the infinite lattice limit, whose corresponding Goldstone modes are the quasicrystalline phasonic degrees of freedom. We show that due to this continuous symmetry and despite the apparent discrete nature of the model, a topological phase transition from a quasi-long-range ordered to a disordered phase occurs at a finite temperature, driven by vortex proliferation. We argue that some of the results are universal properties of two-dimensional systems whose ground state is a quasicrystalline state.

I. INTRODUCTION

While the existence of quasicrystals [1,2] in nature is no longer debatable, it remains an open question if materials can have a quasicrystalline ground state, and what the finite-temperature properties of this phase are [3]. In addition, the characteristics of the phasonic degrees of freedom in quasicrystals are still the focus of much interest [4,5]. It is therefore of great value to investigate the finite-temperature physical properties of simple models with a quasicrystalline ground state. Such models can easily be constructed using the mathematical theory of tilings [6], and have been extensively used for the study of quasicrystallinity [7–10]. In particular, some finite-temperature properties were studied using tiling models. For example, the elastic properties of a three-dimensional model were shown to change upon a finite-temperature phase transition [11,12], and a two-dimensional (2D) tiling model was recently shown to undergo a series of phase transitions leading from the quasicrystalline phase to the liquid phase through a number of intermediate periodic phases [13].

The model studied here is based on the 16 Ammann tiles, each of which is decorated with one label (out of a possible six) on each of its four edges (Fig. 1). Ammann [6] showed that these tiles can perfectly tile the plane such that adjacent edges have matching labels. All such domino-like tiling configurations are nonperiodic and share a quasicrystalline order: well-defined Bragg peaks are observed in the Fourier transform of the densities of each given tile type at frequencies incommensurate with the reciprocal lattice vectors. For an infinite system, there is an uncountable number of different perfect tiling configurations, parameterized by two continuous phases, $\chi_1, \chi_2 \in [0,1)$ (see Appendix A). These phases [14,15] are related to the amplitudes of the Bragg peaks [see Eq. (2) below]. For any finite patch of a perfect tiling, these phases are not well defined and can be described by fuzzy angles, whose uncertainty is inversely proportional to the linear size L [16]. The number of different tilings of a finite system scales linearly with $N = L^2$. Accordingly, a finite change of χ_1 and χ_2 is required in order to induce any change in a finite patch tiling. However, a continuous change of χ_1 and χ_2 induces a continuous change in the *infinite* configuration: the fraction of tiles modified by an infinitesimal change of these phases is linear in this change

---

(Fig. 2). This hidden continuous symmetry of the perfect tilings is therefore manifestly nonlocal. In what follows, we show that this global continuous symmetry has a major impact on the finite-temperature behavior of the model studied here. Namely, like a truly local continuous symmetry, it does not allow the system to be ordered at any positive temperature.

In order to study the model at a finite temperature, one needs to define the Hamiltonian. A natural choice, introduced by Leuzzi and Parisi [17], is to identify the energy of a configuration with the number of mismatching edges. Thus, the (uncountably degenerate) ground states of the model are the perfect tilings exhibiting quasicrystalline order. We wish to study the stability of this order to thermal fluctuations. In order to write the Hamiltonian in a convenient form, we define the 16-dimensional density vector $\vec{\rho}$, containing the 16 tile densities $\rho_i(\mathbf{r})$, each of which is a unity if the tile at $\mathbf{r}$ is of type i, and zero otherwise. In terms of these, the Hamiltonian takes the form

$$H = \sum_{\mathbf{r}} [\vec{\rho}^{\,\dagger}(\mathbf{r})Y\vec{\rho}(\mathbf{r}+\hat{\mathbf{y}}) + \vec{\rho}^{\,\dagger}(\mathbf{r})X\vec{\rho}(\mathbf{r}+\hat{\mathbf{x}})], \quad (1)$$

where X and Y are known interaction matrices, dictated by the above edge-matching rule, whose explicit form can be found in Appendix B. The unit vectors $\hat{\mathbf{x}}$ and $\hat{\mathbf{y}}$ connect each site to (two of) its nearest neighbors. Note that the lattice constant is chosen as the length unit.

Note that in a general quasicrystalline system, two kinds of gapless collective excitations exist: phonons and phasons [15,18]. Phonons describe locally uniform translations, while phasons describe correlated rearrangements of atoms. Our model is defined on a fixed lattice and therefore the low-energy excitations described by this model are the phasonic degrees of freedom.

Previous works [16,17,19] have provided numerical evidence that the model undergoes a symmetry breaking phase transition from a quasicrystalline low-temperature phase into a high-temperature disordered phase. This seems to contradict the well-known Mermin-Wagner theorem, stating that continuous symmetries cannot be spontaneously broken in 2D (or one-dimensional) systems [20–22]. However, the theorem relies on the existence of a *local* order parameter field that can be changed continuously. In our case, each tile, and even the ground state of each finite patch, has a finite degeneracy and cannot be changed continuously. A slow gradient of χ_1 and χ_2 will not make any change in most finite patches of the system,

---

*Current address: Department of Condensed Matter Physics, Weizmann Institute of Science, Rehovot 76100, Israel.
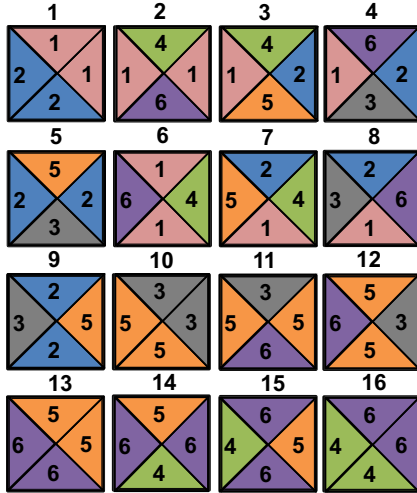
FIG. 1. (Color online) The 16 Ammann tiles.

and will be manifested by a discrete jump in the energy for some isolated patches. It is therefore not clear whether the Mermin-Wagner theorem applies here.

II. ABSENCE OF QUASICRYSTALLINE ORDER

We first provide an argument that quasicrystallinity is broken at any finite temperature, in a fashion similar to the case of a truly continuous local symmetry. For this purpose, we assume that the system is ordered at low temperatures, and self-consistently calculate its finite-temperature properties. It is then shown that thermal excitations destroy the order.

The global symmetry is reflected in the Fourier transform of the tile densities. At a ground state characterized by the two phases χ_1, χ_2, the Fourier transform of $\overrightarrow{\rho}(\mathbf{r})$, $\overrightarrow{\psi}(\mathbf{q})$ takes the form

$$\overrightarrow{\psi}(\mathbf{q}) = N \sum_{m,n,i,j} \delta[\mathbf{q} - 2\pi(n\tau\hat{\mathbf{x}} + m\tau\hat{\mathbf{y}} + i\hat{\mathbf{x}} + j\hat{\mathbf{y}})]$$
$$\times e^{2\pi i(n\chi_1 + m\chi_2)}\overrightarrow{\psi_0}(n,m), \quad (2)$$

where χ_1 and χ_2 are the continuous phases discussed above, $\tau = \frac{\sqrt{5}-1}{2}$ is the inverse golden ratio, and $\overrightarrow{\psi_0}(n,m)$ are

analytically calculated constant amplitudes (see Appendix C). Note that $\mathbf{q}$ is defined modulo reciprocal lattice vectors $G = 2\pi(i\hat{\mathbf{x}} + j\hat{\mathbf{y}})$. Bragg peaks are thus spanned by four independent basis reciprocal vectors (like the closely related square Fibonacci tiling [23]), consistent with the quasicrystalline nature of the model.

Assuming low-temperature quasicrystalline order, only long wavelength excitations should be considered. At scales smaller than the typical wavelength of the contributing excitations, the system appears ordered, slowly passing from one local ground state to another. To express this idea formally, we define the local Fourier transform of a function $f(\mathbf{x})$ as

$$f(\mathbf{x},\mathbf{k}) = \frac{1}{A} \sum_{\mathbf{x}'} f(\mathbf{x}')e^{-i\mathbf{k}\cdot\mathbf{x}'}w_\sigma(\mathbf{x} - \mathbf{x}'), \quad (3)$$

where w_σ is a weight function with a finite length scale σ and $A = \sum_{\mathbf{x}} w_\sigma(\mathbf{x})$. This weight function makes sure that we take only contributions around the point $\mathbf{x}$. In order to simplify the analysis, we take w_σ to be unity in some region with a length scale $\sigma \gg 1$ around the origin, and zero otherwise. As long as σ is large enough, the shape of this region is not important.

We now consider long wavelength excitations where $\chi_1(\mathbf{r})$ and $\chi_2(\mathbf{r})$ change slowly with $\mathbf{r}$, being approximately constant on length scale σ. As the system appears locally ordered, its local Fourier transform is

$$\overrightarrow{\psi}(\mathbf{q}) = N \sum_{m,n,i,j} \delta[\mathbf{q} - 2\pi(n\tau\hat{\mathbf{x}} + m\tau\hat{\mathbf{y}} + i\hat{\mathbf{x}} + j\hat{\mathbf{y}})]$$
$$\times e^{2\pi i(n\chi_1(\mathbf{r})+m\chi_2(\mathbf{r}))}\overrightarrow{\psi_0}(n,m), \quad (4)$$

where $\chi_1(\mathbf{r})$ and $\chi_2(\mathbf{r})$ are the phases corresponding to the local ground state. In terms of the local Fourier transform, the Hamiltonian [Eq. (1)] then takes the form

$$H = \sum_{\mathbf{r},\mathbf{k}} [\overrightarrow{\psi}^\dagger(\mathbf{r},\mathbf{k})Y\overrightarrow{\psi}(\mathbf{r}+\hat{\mathbf{y}},\mathbf{k})e^{ik_y}$$
$$+ \overrightarrow{\psi}^\dagger(\mathbf{r},\mathbf{k})X\overrightarrow{\psi}(\mathbf{r}+\hat{\mathbf{x}},\mathbf{k})e^{ik_x}]. \quad (5)$$

For a locally ordered configuration, one can plug in the local ground state approximation, given by Eq. (4), and get the
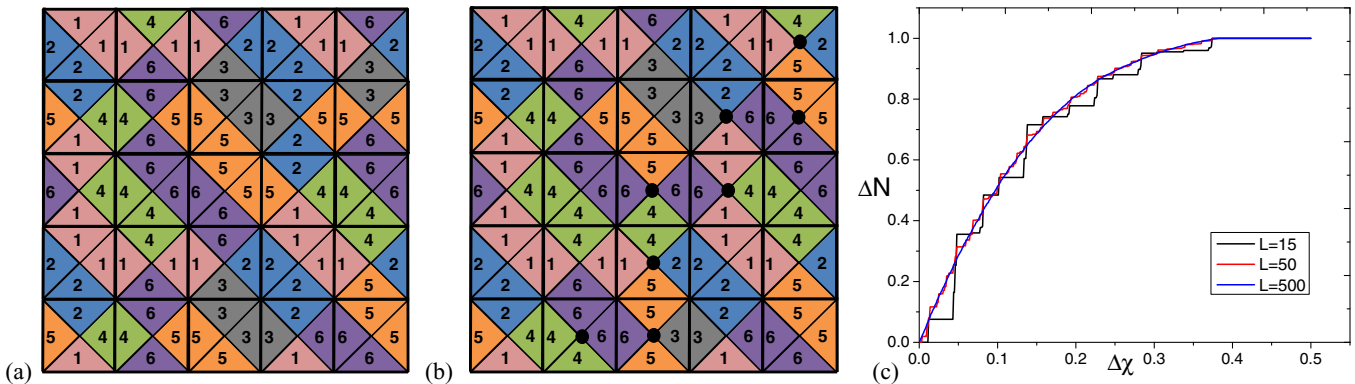

FIG. 2. (Color online) (a) A perfect tiling configuration on a 5×5 lattice generated with $\chi_1 = 0.35$ and $\chi_2 = 0.6$. (b) The minimal change of χ_2 required to change the 5×5 configuration shown in (a) is ~ 0.037 leading to this tiling. The black dots at the center of the tiles denote tiles that are changed in comparison with the configuration shown in (a). (c) ΔN, the fraction of changed tiles as a function of the change $\Delta\chi$ of χ_2, with respect to the configuration $\chi_1 = 0.35, \chi_2 = 0.3$.

effective long wavelength Hamiltonian, $E[\chi_1(\mathbf{r}), \chi_2(\mathbf{r})]$,

$$E = \sum_{\mathbf{r}} \sum_{m,n} [e^{2\pi i(n\partial_x \chi_1 + m\partial_x \chi_2)} \overrightarrow{\psi_0^\dagger}(n,m) X \overrightarrow{\psi_0}(n,m) e^{i2\pi n\tau}$$
$$+ e^{2\pi i(n\partial_y \chi_1 + m\partial_y \chi_2)} \overrightarrow{\psi_0^\dagger}(n,m) Y \overrightarrow{\psi_0}(n,m) e^{i2\pi m\tau}], \quad (6)$$

where $\partial_x \chi_i = \chi_i(\mathbf{r} + \hat{\mathbf{x}}) - \chi_i(\mathbf{r})$ and $\partial_y \chi_i = \chi_i(\mathbf{r} + \hat{\mathbf{y}}) - \chi_i(\mathbf{r})$ are the discrete derivatives of χ_i. The sums over m and n can be performed numerically, and the final result, to lowest order in the derivatives, is

$$E = \sum_{\mathbf{r}} A(|\partial_x \chi_1| + |\partial_y \chi_2|) + B(|\partial_x \chi_2| + |\partial_y \chi_1|)$$
$$+ C(|\partial_x \chi_1 + \tau \partial_x \chi_2| + |\partial_y \chi_2 + \tau \partial_y \chi_1|)$$
$$+ D(|\partial_y \chi_1 + \tau \partial_y \chi_2| + |\partial_x \chi_2 + \tau \partial_x \chi_1|), \quad (7)$$

where $A \approx 1.00$, $B \approx 1.94$, $C \approx 1.57$, and $D \approx 0.61$.

We now investigate this effective Hamiltonian at finite temperatures. Once we rephrase the low-T physics of the model in terms of truly continuous fields, it is rather obvious that the Mermin-Wagner theorem applies, and thermal excitations must destroy the order in any finite temperature. However, three notes are in order. First, note that the Mermin-Wagner theorem holds even though the effective field theory is nonanalytic, as long as it is continuous [24]. Second, the transformation from the tiles degrees of freedom to the continuous phases involves a nontrivial, singular Jacobian, which at finite temperature translates into a complicated entropic term. While this entropic term remains unspecified, it must preserve the continuous symmetry in the local ground state approximation, and therefore should not affect our argument. Third, as discussed above, the local phases are never truly continuous. Each finite patch of the system has a finite ground state degeneracy, and thus the number of distinct values that any of the phases can take is finite and scales like the patch size σ, which can be taken to be the largest scale over which the system is in an approximate ground state. However, here one can invoke the discrete tile picture of the system: as any mismatch in a tiling costs at least one unit of energy, the density of mismatches at low temperatures is, at most, $O[\exp(-\Delta/T)]$, with Δ of order unity. Thus, σ, i.e., the scale upon which the system is at a local ground state, can be made exponentially large as temperature decreases, and the system can be effectively described by continuous phases. The assumption of low-temperature order leads to a contradiction, and the system is therefore not ordered at any finite temperature.

The transition found in [16,17,19] is therefore not a symmetry breaking transition. We now turn to investigate its true nature.

III. FINITE-TEMPERATURE BEHAVIOR OF THE MODEL

A natural choice for the order parameters of the model, closely related to the one defined in [19], is the Fourier coefficients of the tile densities at the basis reciprocal vectors:

$$q_i^x = \frac{1}{N} \sum_{\mathbf{r}} e^{-i2\pi \tau x} \rho_i(\mathbf{r}), \quad q_i^y = \frac{1}{N} \sum_{\mathbf{r}} e^{-i2\pi \tau y} \rho_i(\mathbf{r}), \quad (8)$$

where i is one of the 16 tile types, and its choice is arbitrary. Note the need for two order parameters, as the ground state

manifold is parameterized by two phases. While this form is correct, a more symmetric and numerically preferable generalization is

$$Q_x = \frac{1}{N} \sum_{i,\mathbf{r}} e^{-i2\pi \tau x} e^{i\gamma_i^x} \rho_i(\mathbf{r}), \quad Q_y = \frac{1}{N} \sum_{i,\mathbf{r}} e^{-i2\pi \tau y} e^{i\gamma_i^y} \rho_i(\mathbf{r}), \quad (9)$$

which sums the contribution from all tile types i. The phases γ_i^x and γ_i^y are the relative phases between the Bragg peaks amplitudes observed for each tile type (see Appendix C). We measured these order parameters in the vicinity of the transition ($T_c \simeq 0.418$) and below it, using Monte Carlo simulations of the *original tiling model*. Ground state configurations are nearly periodic with periodicities that are Fibonacci numbers (see Appendix A). We found that finite size effects are minimized using periodic boundary conditions, provided linear system size is a Fibonacci number.

Well below the transition, $|Q|^2 \propto L^{-\eta(T)}$ (Fig. 3), implying a power-law decay of the correlation function with the same exponent $\eta(T)$. Above the transition, $|Q|^2$ falls exponentially, indicating short-range correlations. This resembles the situation in the XY model, for example, which exhibits a quasi-long-range order (QLRO) at low-T and a topological Kosterlitz-Thouless (KT) transition [25,26] to a disordered phase.

The KT transition is associated with vortex unbinding. It is therefore natural to ask whether single vortices become stable at high temperatures in our system. A vortex in the field χ_1, for example, is given by a configuration associated with

$$\chi_1 = \frac{1}{2\pi} \arctan \frac{y}{x}, \quad \chi_2 = 0. \quad (10)$$

Using Eq. (7), it is easy to see that the energy of the vortex diverges, $H_{\text{vortex}} \propto L$. The positional entropy of the vortex, on the other hand, grows with the system's size only as $\log L$. A naive application of the standard KT argument, explaining the onset of vortex unbinding as a consequence of the positional entropy overcoming the energy, would lead to the conclusion
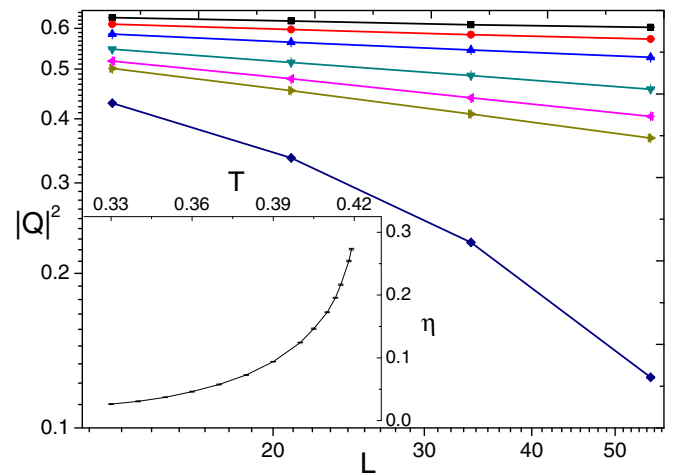

FIG. 3. (Color online) $|Q|^2 = \frac{1}{2}(|Q_x|^2 + |Q_y|^2)$ as a function of the system's size at different temperatures (top to bottom: $T = 0.34, 0.36, 0.38, 0.4, 0.41, 0.415, 0.43$). Note the log-log scale. For T very close but higher than $T_c \sim 0.42$, an exponential decay is evident. Inset: η as a function of T below the critical temperature.
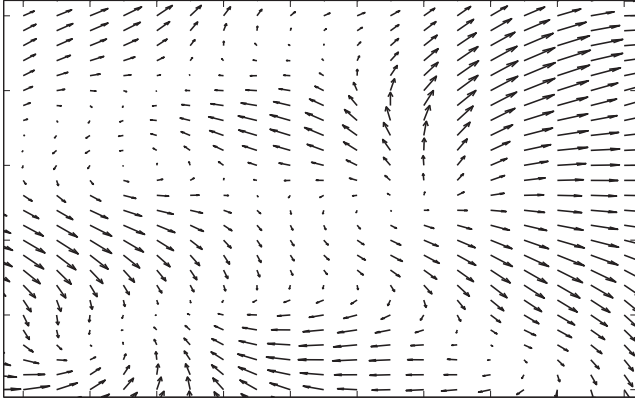
FIG. 4. A typical configuration above the transition. The arrows represent the complex numbers $\psi_1(\mathbf{r}, 2\pi\tau\hat{\mathbf{x}})$ with $w_\sigma = \exp(-r^2/\sigma^2)$ and $\sigma = 5$. We note that vortices similar to those shown in the figure were observed in all of the configurations above T_c. Below T_c, no vortices were observed.

that in our case energy always wins and vortices are never stable. This conclusion is clearly wrong—our transition is associated with proliferation of vortices; see Fig. 4. Upon integrating out the fast degrees of freedom, the field theory (7) is likely to be renormalized into an effective Gaussian free-energy functional, which results in a logarithmically diverging vortex effective energy. This was shown to be the case for a similar tiling model at any finite temperature [27]. The standard KT argument for positional entropy overcoming the *effective* free energy of the vortex at high temperatures does hold, and vortex unbinding will drive a topological phase transition.

In the usual KT scenario, where the energy itself is quadratic to lowest order, $\eta \propto T$ at low temperatures. In contrast, in our case, η shows a highly nonlinear behavior (Fig. 3, inset). This too signals that the effective coupling constant is strongly renormalized and becomes temperature dependent. The very steep decay of η as one moves away from the transition implies that in finite lattices at low temperatures, the system appears to be ordered, and the identification of the algebraic correlations is very difficult in reasonably sized systems. This explains why previous works [16,17,19] identified the low-temperature phase as an ordered one.

However, one feature of our transition deviates from the KT scenario. At the KT transition, the heat capacity C_v exhibits a weak (numerically undetectable) C_∞ essential singularity. As shown in [16,17,19], the tiling model exhibits a distinctive sharp peak in C_v at T_c. In particular, we observed (for L up to 89) a clear power-law divergence, $.\frac{dC_v}{dT}|_{T_C} \propto L^{-\varepsilon}$, with ε (very roughly) $\sim$0.5(3), indicating a finite-order transition with $\nu \simeq 1.25(20)$. Bearing in mind the large uncertainties in these numerical estimates and the limited system sizes, this seems to suggest our transition may be of a different universality class than the standard KT transition. A qualitative change in critical behavior due to interaction between two XY fields was pointed out in the context of a double-layer XY model [28].

It is worth saying a few words about the form of the long wavelength Hamiltonian, given by Eq. (7). Usually, only analytic terms are considered when one constructs an effective field theory. The tiling model provides an example where nonanalytic terms arise naturally from first principles.

In fact, it was already suggested that terms of the form $\sim |\partial\chi|$ describe the energy of phasons in general systems with a quasicrystalline ground state [18]. A phase in which the *free energy* is characterized by such a nonanalytic form is usually referred to as a locked phase [8]. In 3D, one expects to find a finite-temperature transition from this phase to an unlocked phase, characterized by a quadratic free energy [11,12]. However, in 2D systems, such as the one studied in this work, the transition occurs at zero temperature, as was shown in [27]. A similar derivation of the energy can be made for an analog three-dimensional system, where we expect that the equivalent of (7) would be the relevant low-temperature effective theory.

IV. CONCLUSIONS

We described here a topological phase transition in a system with discrete degrees of freedom. It is constructive to juxtapose this behavior with a similar scenario. The clock model, where each spin can take one of q possible planar directions [29–31], exhibits a KT transition for $q > 4$. In this case, as long as $k_B T$ exceeds the energy of rotating a single spin between two neighboring directions, thermal fluctuations restore the continuous U(1) symmetry and one effectively gets back an XY model with algebraically decaying correlations. Indeed, as temperature decreases, the discrete nature is revealed and a second phase transition occurs below which the system is ordered. In comparison, in our tiling model, the hidden continuous U(1) symmetry is restored not by temperature but rather by going into larger and larger finite-ordered patches. The lower the temperature, the larger are the ordered patches in the system, and thus the QLRO phase survives for arbitrarily low temperatures. Given that the continuous symmetry discussed here is a general property of quasicrystals, similar arguments may lead to the conclusion that any 2D model with a quasicrystalline ground state (with either discrete or continuous degrees of freedom) cannot be ordered at any positive temperature. Indeed, algebraic correlations (but not a KT transition) were observed in a Penrose tiling model [27] and various random tiling models [8], and we expect the tiling model recently studied by Nikola *et al.* [13] to exhibit QLRO at low temperatures as well. Furthermore, in our model, rotational symmetry is explicitly broken by the underlying real-space lattice. However, the above formulation of the configuration in terms of the local phases enables one to study, in off-lattice models, the orientational QLRO of these fields. One expects a two-step melting of the QLRO quasicrystal through an intermediate "hexatic" (or, rather, "pentatic" for a fivefold symmetric quasicrystal) phase, as was predicted in [32].

APPENDIX A: GENERATING GROUND STATE CONFIGURATIONS AND EXCITATIONS

For many purposes (some of which will be mentioned soon), it is necessary to generate a configuration with given χ_1 and χ_2. In what follows, we show how this can be done. Motivated by the connection between our model and the square
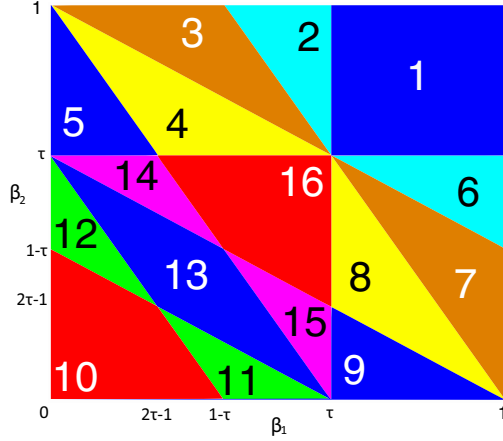
FIG. 5. (Color online) The mapping between the $\beta_1 - \beta_2$ torus and the 16 tile types.

Fibonacci sequence [16], we define the two functions

$$\beta_1(\mathbf{r}) = \{\chi_1 + \tau x\}, \quad \beta_2(\mathbf{r}) = \{\chi_2 + \tau y\}, \tag{A1}$$

where $\{\cdots\}$ is the fractional part of $\cdots$, i.e., $(\cdots)\mathrm{mod}\,1$. In a perfect tiling, each tile type is associated with a given region on the $\beta_1 - \beta_2$ torus (Fig. 5). Together with Eq. (A1), this mapping allows for generating a perfect tiling

for an arbitrary choice of χ_1 and χ_2. In order to study the excitations within the local ground state approximation, one may now construct nonperfect configurations with slowly varying phases: $\beta_1(\mathbf{r}) = \{\chi_1(\mathbf{r}) + \tau x\}, \beta_2(\mathbf{r}) = \{\chi_2(\mathbf{r}) + \tau y\}$. Looking at the associated nonperfect tiling configuration, it is possible to verify numerically that their energy follows the relation

$$
\begin{aligned}
E = \sum_{\mathbf{r}} & A(|\partial_x \chi_1| + |\partial_y \chi_2|) + B(|\partial_x \chi_2| + |\partial_y \chi_1|) \\
& + C(|\partial_x \chi_1 + \tau \partial_x \chi_2| + |\partial_y \chi_2 + \tau \partial_y \chi_1|) \\
& + D(|\partial_y \chi_1 + \tau \partial_y \chi_2| + |\partial_x \chi_2 + \tau \partial_x \chi_1|),
\end{aligned}
\tag{A2}
$$

which was derived in the main text (to lowest order in derivatives).

Using this explicit tiling construction, it is easy to see the near periodicities of the perfect tiling configurations. Fibonacci numbers satisfy $\tau F_n \simeq F_{n-1}$ (for large n), and thus $\beta_1(x, y) \simeq \beta_1(x + F_n, y)$ and $\beta_2(x, y) \simeq \beta_2(x, y + F_n)$.

APPENDIX B: EXPLICIT FORM OF *X* AND *Y*

The matrices X and Y used to define the Hamiltonian (1) are derived directly from the matching rules and the definition of the 16 tiles found in Fig. 1. Their explicit form is

$$
Y = \begin{pmatrix}
1 & 1 & 1 & 1 & 1 & 1 & 0 & 0 & 0 & 1 & 1 & 1 & 1 & 1 & 1 & 1 \\
1 & 1 & 1 & 0 & 1 & 1 & 1 & 1 & 1 & 1 & 1 & 1 & 1 & 1 & 0 & 0 \\
1 & 1 & 1 & 1 & 0 & 1 & 1 & 1 & 1 & 1 & 1 & 0 & 0 & 0 & 1 & 1 \\
1 & 1 & 1 & 1 & 1 & 1 & 1 & 1 & 1 & 0 & 0 & 1 & 1 & 1 & 1 & 1 \\
1 & 1 & 1 & 1 & 1 & 1 & 1 & 1 & 1 & 0 & 0 & 1 & 1 & 1 & 1 & 1 \\
0 & 1 & 1 & 1 & 1 & 0 & 1 & 1 & 1 & 1 & 1 & 1 & 1 & 1 & 1 & 1 \\
0 & 1 & 1 & 1 & 1 & 0 & 1 & 1 & 1 & 1 & 1 & 1 & 1 & 1 & 1 & 1 \\
0 & 1 & 1 & 1 & 1 & 0 & 1 & 1 & 1 & 1 & 1 & 1 & 1 & 1 & 1 & 1 \\
1 & 1 & 1 & 1 & 1 & 1 & 0 & 0 & 0 & 1 & 1 & 1 & 1 & 1 & 1 & 1 \\
1 & 1 & 1 & 1 & 0 & 1 & 1 & 1 & 1 & 1 & 1 & 0 & 0 & 0 & 1 & 1 \\
1 & 1 & 1 & 0 & 1 & 1 & 1 & 1 & 1 & 1 & 1 & 1 & 1 & 1 & 0 & 0 \\
1 & 1 & 1 & 1 & 0 & 1 & 1 & 1 & 1 & 1 & 1 & 0 & 0 & 0 & 1 & 1 \\
1 & 1 & 1 & 0 & 1 & 1 & 1 & 1 & 1 & 1 & 1 & 1 & 1 & 1 & 0 & 0 \\
1 & 0 & 0 & 1 & 1 & 1 & 1 & 1 & 1 & 1 & 1 & 1 & 1 & 1 & 1 & 1 \\
1 & 1 & 1 & 0 & 1 & 1 & 1 & 1 & 1 & 1 & 1 & 1 & 1 & 1 & 0 & 0 \\
1 & 0 & 0 & 1 & 1 & 1 & 1 & 1 & 1 & 1 & 1 & 1 & 1 & 1 & 1 & 1
\end{pmatrix},
$$

$$
X = \begin{pmatrix}
1 & 1 & 0 & 0 & 0 & 1 & 1 & 1 & 1 & 1 & 1 & 1 & 1 & 1 & 1 & 1 \\
0 & 0 & 1 & 1 & 1 & 1 & 1 & 1 & 1 & 1 & 1 & 1 & 1 & 1 & 1 & 1 \\
0 & 0 & 1 & 1 & 1 & 1 & 1 & 1 & 1 & 1 & 1 & 1 & 1 & 1 & 1 & 1 \\
0 & 0 & 1 & 1 & 1 & 1 & 1 & 1 & 1 & 1 & 1 & 1 & 1 & 1 & 1 & 1 \\
1 & 1 & 0 & 0 & 0 & 1 & 1 & 1 & 1 & 1 & 1 & 1 & 1 & 1 & 1 & 1 \\
1 & 1 & 1 & 1 & 1 & 1 & 1 & 0 & 1 & 1 & 1 & 1 & 1 & 0 & 1 & 0 \\
1 & 1 & 1 & 1 & 1 & 1 & 1 & 1 & 0 & 1 & 0 & 1 & 0 & 1 & 0 & 1 \\
1 & 1 & 1 & 1 & 1 & 1 & 1 & 1 & 1 & 0 & 1 & 0 & 1 & 1 & 1 & 1 \\
1 & 1 & 1 & 1 & 1 & 1 & 1 & 1 & 1 & 0 & 1 & 0 & 1 & 1 & 1 & 1 \\
1 & 1 & 1 & 1 & 1 & 1 & 1 & 1 & 0 & 1 & 0 & 1 & 0 & 1 & 0 & 1 \\
1 & 1 & 1 & 1 & 1 & 1 & 1 & 1 & 0 & 1 & 0 & 1 & 0 & 1 & 0 & 1 \\
1 & 1 & 1 & 1 & 1 & 1 & 1 & 0 & 1 & 1 & 1 & 1 & 1 & 0 & 1 & 0 \\
1 & 1 & 1 & 1 & 1 & 1 & 1 & 0 & 1 & 1 & 1 & 1 & 1 & 0 & 1 & 0 \\
1 & 1 & 1 & 1 & 1 & 1 & 1 & 0 & 1 & 1 & 1 & 1 & 1 & 0 & 1 & 0 \\
1 & 1 & 1 & 1 & 1 & 0 & 0 & 1 & 1 & 1 & 1 & 1 & 1 & 1 & 1 & 1 \\
1 & 1 & 1 & 1 & 1 & 0 & 0 & 1 & 1 & 1 & 1 & 1 & 1 & 1 & 1 & 1
\end{pmatrix}.
$$

TABLE I. The phases needed to define the order parameters Q_x and Q_y.

m	1	2	3	4	5	6	7	8
$\gamma_m^y/2\pi$	0.8090	0.8756	0.8756	0.7424	0.7424	0.5400	0.3368	0.2812
$\gamma_m^x/2\pi$	0.8090	0.5400	0.3368	0.2812	0.0780	0.8756	0.8756	0.7424
m	9	10	11	12	13	14	15	16
$\gamma_m^y/2\pi$	0.0780	0.1403	0.0780	0.4113	0.3090	0.5400	0.20968	0.4778
$\gamma_m^x/2\pi$	0.7424	0.1403	0.4113	0.0780	0.3090	0.2068	0.5400	0.4778

APPENDIX C: FOURIER COMPONENTS

Here we show how to calculate the Fourier components of the tile densities in a ground state configuration. The discrete Fourier transform of tile number l at the reciprocal vector $\mathbf{G} = 2\pi\tau\,(n\hat{\mathbf{x}} + m\hat{\mathbf{y}})$ is

$$\psi_l(n,m) = \frac{1}{N} \sum_{\mathbf{r}} \rho_l(\mathbf{r}) e^{-i2\pi\tau nx} e^{-i2\pi\tau my}. \quad (C1)$$

Using the definitions of β_1 and β_2, we can write

$$\psi_l(n,m) = e^{2\pi in\chi_1} e^{2\pi im\chi_2} \frac{1}{N} \sum_{\mathbf{r}} \rho_l(\mathbf{r}) e^{-i2\pi n\beta_1} e^{-i2\pi m\beta_2}. \quad (C2)$$

We define Ω_l as the region associated with tile number l in the $\beta_1 - \beta_2$ torus, defined in Fig. 5. As τ is irrational, the functions β_1 and β_2 cover the region Ω_l densely and uniformly, and the infinite sum in (C2) can be turned into an integral:

$$\psi_l(n,m) = e^{2\pi in\chi_1} e^{2\pi im\chi_2} \iint_{\Omega_l} d\beta_1 d\beta_2 e^{-i2\pi n\beta_1} e^{-i2\pi m\beta_2}. \quad (C3)$$

This integral can be performed analytically, and we can now find the Fourier components. As an example, let us calculate the Fourier transform of tile number 2:

$$\psi_2(n,m) = e^{2\pi in\chi_1} e^{2\pi im\chi_2} \iint_{\Omega_2} d\beta_1 d\beta_2 e^{-i2\pi n\beta_1} e^{-i2\pi m\beta_2}$$

$$= e^{2\pi in\chi_1} e^{2\pi im\chi_2} \int_\tau^1 d\beta_1 \int_{1-\tau\beta_1}^\tau d\beta_2 e^{-i2\pi n\beta_1} e^{-i2\pi m\beta_2}$$

$$= -e^{2\pi in\chi_1} e^{2\pi im\chi_2}$$

$$\times \frac{im\sin 2\pi n\tau + in\tau e^{2\pi i\tau(n+\frac{m}{2})}\sin\pi m\tau}{2mn\pi^2(m-\tau n)}. \quad (C4)$$

Using Parseval's theorem, one can now check that, indeed, the components corresponding to the reciprocal vectors $\mathbf{G} = 2\pi\tau\,(n\hat{\mathbf{x}} + m\hat{\mathbf{y}})$ are the only nonvanishing components. The diffraction pattern is therefore composed of δ peaks, which confirms the quasicrystalline nature of each perfect tiling.

Having found a general way to calculate the Fourier components of the ground state, we now define the phases γ_m^x and γ_m^y (used for the definition of the order parameters Q_x and Q_y in the main text). We chose the phases such that contributions of all tile types to the Bragg peak amplitudes will add coherently in a ground state. The Fourier components at $\mathbf{G} = 2\pi\tau\hat{\mathbf{x}}$ can be found using Eq. (C3). Writing them in the form $\psi_m(1,0) = |\psi_m(1,0)|\, e^{i\zeta_m}$, it is easy to see that the order parameter will have the largest possible length if the phases γ_m are chosen to be $-\zeta_m$. The same procedure can be used to find the phases corresponding to $\mathbf{G} = 2\pi\tau\hat{\mathbf{y}}$. The phases ζ_m^x and ζ_m^y correspond to the center of mass of the region Ω_m on the $\beta_1 - \beta_2$ torus. Table I gives the phases γ_m of the two order parameters.

[1] D. Shechtman, I. Blech, D. Gratias, and J. W. Cahn, Phys. Rev. Lett. **53**, 1951 (1984).

[2] D. Levine and P. J. Steinhardt, Phys. Rev. Lett. **53**, 2477 (1984).

[3] M. de Boissieu, Chem. Soc. Rev. **41**, 6778 (2012).

[4] M. Widom, Philos. Mag. **88**, 2339 (2008).

[5] J. A. Kromer, M. Schmiedeberg, J. Roth, and H. Stark, Phys. Rev. Lett. **108**, 218301 (2012).

[6] B. Grunbaum and G. C. Shephard, *Tilings and Patterns* (Freeman, New York, 1986).

[7] *Physical Properties of Quasicrystals*, edited by Z. M. Stadnik (Springer, Berlin, 1999).

[8] *Quasicrystals: The State of the Art*, edited by Paul J. Steinhardt and D. P. Divincenzo (World Scientific, Singapore, 1999).

[9] *Quasicrystals: An Introduction to Structure, Physical Properties and Applications*, edited by J. B. Suck, M. Schreiber, and P. Hussler (Springer, Berlin, 2002).

[10] *Quasicrystals: Structure and Physical Properties*, edited by H.-R. Trebin (Wiley-VCH, Weinheim, 2006).

[11] H. C. Jeong and P. J. Steinhardt, Phys. Rev. B **48**, 9394 (1993).

[12] T. Dotera and P. J. Steinhardt, Phys. Rev. Lett. **72**, 1670 (1994).

[13] N. Nikola, D. Hexner, and D. Levine, Phys. Rev. Lett. **110**, 125701 (2013).

[14] N. Mermin, Rev. Mod. Phys. **64**, 3 (1992).

[15] R. Lifshitz, Isr. J. Chem. **51**, 1156 (2011).

[16] H. Koch and C. Radin, J. Stat. Phys. **138**, 465 (2009).

[17] L. Leuzzi and G. Parisi, J. Phys. A **33**, 4215 (2000).

[18] J. E. S. Socolar, T. C. Lubensky, and P. J. Steinhardt, Phys. Rev. B **34**, 3345 (1986).

[19] Z. Rotman and E. Eisenberg, Phys. Rev. E **83**, 011123 (2011).

[20] N. D. Mermin and H. Wagner, Phys. Rev. Lett. **17**, 1133 (1966).

[21] P. Hohenberg, Phys. Rev. **158**, 383 (1967).

[22] N. Mermin, Phys. Rev. **176**, 250 (1968).

[23] R. Lifshitz, J. Alloys Compd. **342**, 186 (2002).

[24] D. Ioffe, S. B. Shlosman, and Y. Velenik, Commun. Math. Phys. **226**, 433 (2002).

[25] J. M. Kosterlitz and D. J. Thouless, J. Phys. C **5**, L124 (1972).

[26] J. M. Kosterlitz, J. Phys. C **7**, 1046 (1974).

[27] L.-H. Tang and M. V. Jarić, Phys. Rev. B **41**, 4524 (1990).

[28] N. Parga and J. van Himbergen, Solid State Commun. **35**, 607 (1980).

[29] J. V. José, L. P. Kadanoff, S. Kirkpatrick, and D. R. Nelson, Phys. Rev. B **16**, 1217 (1977).

[30] S. Elitzur, R. B. Pearson, and J. Shigemitsu, Phys. Rev. D **19**, 3698 (1979).

[31] G. Ortiz, E. Cobanera, and Z. Nussinov, Nucl. Phys. B **854**, 780 (2012).

[32] P. De and R. A. Pelcovits, J. Phys. A: Math. Gen. **22**, 1167 (1989).